

On the Theoretical Framework of Magnetized Outflows from Stellar-Mass Black Holes and Related Observations

D. M. Christodoulou,^{1,2*} I. Contopoulos,^{3,4†} D. Kazanas,^{5‡} J. F. Steiner,^{6§}
D. B. Papadopoulos,^{7¶} and S. G. T. Laycock^{1,8||}

¹Lowell Center for Space Science and Technology, University of Massachusetts Lowell, Lowell, MA, 01854, USA

²Department of Mathematical Sciences, University of Massachusetts Lowell, Lowell, MA, 01854, USA

³Research Center for Astronomy and Applied Mathematics, Academy of Athens, Athens 11527, Greece

⁴National Research Nuclear University, Moscow 115409, Russia

⁵NASA Goddard Space Flight Center, Laboratory for High-Energy Astrophysics, Code 663, Greenbelt, MD 20771, USA

⁶MIT Kavli Institute for Astrophysics and Space Research, Cambridge, MA 02139, USA

⁷Department of Physics, Aristotle University of Thessaloniki, Thessaloniki 54124, Greece

⁸Department of Physics & Applied Physics, University of Massachusetts Lowell, Lowell, MA, 01854, USA

22 June 2016

ABSTRACT

The spins of stellar-mass black holes (BHs) and the power outputs of their jets are measurable quantities. Unfortunately, the currently employed methods do not agree and the results are controversial. Two major issues concern the measurements of BH spin and beam (jet) power. The former issue can be resolved by future observations. But the latter issue can be resolved now, if we pay attention to what is expected from theoretical considerations. The question of whether a correlation has been found between the power outputs of few objects and the spins of their BHs is moot because BH beam power does not scale with the square of the spin of the BH. We show that the theoretical BH beam power is a strongly nonlinear function of spin that cannot be approximated by a quadratic relation, as is generally stated when the influence of the magnetic field is not accounted for in the [Blandford & Znajek \(1977\)](#) model. The BH beam power of ballistic jets should scale a lot more steeply with BH spin irrespective of the magnetic field assumed to thread the horizon and the spin range considered. This behavior may already be visible in the analyses of radio observations by [Narayan & McClintock \(2012\)](#) and [Russell et al. \(2013\)](#). In agreement with previous studies, we also find that the power output that originates in the inner regions of the surrounding accretion disks is higher than that from the BHs and it cannot be ignored in investigations of continuous compact jets from these systems.

Key words: accretion, accretion disks—black hole physics—ISM: jets and outflows—magnetic fields—X-rays: binaries

1 INTRODUCTION

In the past few years, a great deal of effort has been devoted to the study of stellar-mass accreting black holes (BHs) that are members of binary systems with the intention to pinpoint the location of the innermost stable circular orbits (ISCOs) of their accretion disks and to determine the state of rotation of these compact objects. Such

investigations are not easy to undertake as they require high-resolution observations of the few known BH binaries followed by intensive relativistic modeling of the spectral features that arise from the gas orbiting near and accreted by the BHs. Thorough descriptions of the subject and the most accurate results to date can be found in the reviews of [Remillard & McClintock \(2006\)](#), [Miller \(2007\)](#), [McClintock et al. \(2011, 2014\)](#), and [Reynolds \(2014\)](#), as well as in the works of [Fender et al. \(2010\)](#), [Miller et al. \(2011\)](#), [Steiner et al. \(2013, 2014\)](#), [Reid et al. \(2014\)](#), [Orosz et al. \(2014\)](#), [Wu et al. \(2016\)](#), and [Chen et al. \(2016\)](#). In summary:

(a) The continuum-fitting (CF) method is currently a

* E-mail: dimitris_christodoulou@uml.edu

† E-mail: icontop@academyofathens.gr

‡ E-mail: demos.kazanas@nasa.gov

§ E-mail: jsteiner@mit.edu

¶ E-mail: papadop@astro.auth.gr

|| E-mail: silas_laycock@uml.edu

leading method for determining the location of the ISCO of the orbiting gas and from it the BH spin parameter. The CF method uses a model-dependent fit of the thermal continuum X-ray spectrum in low-luminosity systems and requires precise knowledge of the physical state of the inner accretion disk, its inclination, the BH mass, and the distance to the system. Determinations of these parameters have been improving over the years and detailed model fits have produced accurate values of the location of the ISCO and the BH spin for a sample of 10 stellar-mass BHs (McClintock et al. 2006; Shafee et al. 2006; Gou et al. 2009, 2010; Steiner et al. 2010; McClintock et al. 2011; Gou et al. 2011; Steiner et al. 2014; Chen et al. 2016).

(b) The iron $K\alpha$ -line (Fe $K\alpha$) method is an independent method that is also used to determine the locations of the ISCOs in the accretion disks around galactic as well as extragalactic BHs. This method uses a model-dependent fit of the dynamical broadening of the Fe $K\alpha$ emission line that is excited in the inner edge of the accretion disk by external irradiation. The Fe $K\alpha$ method does not require knowledge of the BH mass, the disk inclination, or the distance to the system, and it has also produced accurate values of the location of the ISCO and the BH spin for a sample of about 10 stellar-mass BHs (Blum et al. 2009; Miller et al. 2009; Reis et al. 2009, 2010; Hiemstra et al. 2010; Steiner et al. 2010; Miller et al. 2011; Russell et al. 2013; Reynolds 2014).

At present, seven BHs in X-ray binaries have been analyzed by both methods and the results disagree in the cases of 4U 1543-47 and GRO J1655-40 (Reynolds 2014); and likely in the case of GX 339-4 (Miller et al. 2009; Kolehmainen & Done 2010) for which BH mass, distance, and disk inclination are uncertain (Shaposhnikov & Titarchuk 2009; Özel et al. 2010). In this investigation, we do not intend to examine the differences between the two methods; on the contrary, we need a homogeneous data set of BH masses and spins in order to investigate theoretically the electromagnetic output from such systems. For this reason, we choose to use only data from the CF method which depends on accurate determinations of BH masses, values that we need for our study as well. These data are listed in Table 1 and references are shown in the last column of the table.

Determinations of the ISCOs and the spins of BHs have consistently neglected the effects of the magnetic field that may exist in the inner accretion disks and in the accreted plasma. The rationale behind this assumption is that torques due to the embedded magnetic field at the ISCO can only account for a small correction that lies well within the errors due to modeling of the X-ray continuum in low-luminosity sources ($\ell/\ell_{\text{Edd}} < 0.3$, where ℓ_{Edd} is the Eddington luminosity). As detailed by McClintock et al. (2011), calculations that take magnetic torques into account do not produce systematic errors larger than the observational errors, even for disks with $\ell/\ell_{\text{Edd}} \approx 0.35 - 0.5$.

However, the above efforts to quantify the influence of an embedded magnetic field near the ISCO do not address the problem in its entirety because the power output of jet-like outflows from these systems depends strongly on the magnetic field that can be supported in the region between the ISCO and the event horizon of the

BH (Contopoulos & Papadopoulos 2012; Contopoulos et al. 2016). Furthermore, it is now understood that magnetic field can be generated *in situ* and grow linearly in the inner disks around BHs by the Poynting-Robertson Cosmic Battery (PRCB) (Contopoulos & Kazanas 1998; Contopoulos et al. 2006; Christodoulou et al. 2008), and this mechanism appears to be at work in the vicinities of both supermassive BHs (Contopoulos et al. 2009; Christodoulou et al. 2016) as well as stellar-mass BHs (Kylafis et al. 2012). The PRCB can operate efficiently in the inner accretion disks of stellar-mass compact systems for as long as the accretion flows are advection-dominated (ADAF), and it is capable of building a significant magnetic field of a single polarity in less than 1 day (Kylafis et al. 2012).

Generally speaking, accretion disks around stellar-mass BHs have two “magnetic” states available to them depending on whether their BHs were born with a very high or a low/moderate spin. Because of the extremely long timescales for substantially increasing the spin by accretion (McClintock et al. 2011; Gou et al. 2011), the various compact systems cannot cross over between these two states and the observations should then find them with their ISCOs either near the event horizon or near the nonrotating value (Contopoulos & Papadopoulos 2012). Thus, the result could be a segregation of spins into two broad groups. The data shown in Table 1 already appear to be in agreement with this hypothesis despite the markedly small number of objects involved; there exists only one object with spin a_* (defined in § 2 below) in the intermediate region between 0.34 and 0.70. A similar gap in the a_* interval of 0.3-0.75 is seen in the Fe $K\alpha$ data as well (Fender et al. 2010). For these reasons, we are compelled to analyze the physical properties of the two groups of objects separately and not just as one uniform sample.

In what follows, we describe the theoretical framework for the energetics of jet-like outflows from stellar-mass BH binaries. The expected power output from such systems is analyzed in considerably more detail than previously done (Livio et al. 1999; Meier 1999, 2001). Equipartition between the magnetic pressure and the ram pressure of inflowing matter provides an estimate of the magnetic field that can be supported in the region between the ISCO and the BH horizon (Contopoulos & Kazanas 1998). Then the poloidal magnetic flux and the beam (jet) power are calculated by using the standard equations provided by classical theories of emission from the BH and the inner accretion disk (Blandford & Znajek 1977; Blandford & Payne 1982; Contopoulos & Lovelace 1994; Livio et al. 1999; Meier 1999, 2001). In § 2, we analyze jet emission only from the vicinity of the BH. In § 3, we add the contribution from a nonrelativistic disk to the results of § 2. In § 4, we repeat the calculations using a new estimate of the maximum supported magnetic field inside the ISCO (Contopoulos et al. 2016). We conclude in § 5 with a summary and a discussion of our results.

2 ELECTROMAGNETIC OUTPUT FROM THE BLACK HOLE

We determine the poloidal magnetic flux Ψ_{BH} and the power output L_{BH} in the vicinity of a BH. Metric-system units

Table 1. Spin Parameters from the CF Method and Masses of Stellar-Mass Black Holes

No.	Object	a_*	M/M_\odot	References
1	Cygnus X-1	>0.99	14.8 (± 1.0)	1, 2
2	GRS 1915+105	>0.98	12.4 ($+2.0, -1.8$)	3, 11
3	LMC X-1	0.92 ($+0.05, -0.07$)	10.91 (± 1.54)	4
4	M33 X-7	0.84 (± 0.05)	15.65 (± 1.45)	5
5	4U 1543-47	0.80 (± 0.05)	9.4 (± 1.0)	6
6	GRO J1655-40	0.70 (± 0.05)	6.30 (± 0.27)	6
7	Nova Mus '91	0.63 (± 0.18)	11.0 ($+2.1, -1.4$)	12, 13
8	XTE J1550-564	0.34 ($+0.20, -0.28$)	9.10 (± 0.61)	7
9	LMC X-3	0.25 (± 0.15)	7.0 (± 0.6)	8, 10, 14, 15
10	A0620-00	0.12 (± 0.19)	6.61 (± 0.25)	9

Ref. Key: 1–Orosz et al. (2011), 2–Gou et al. (2011), 3–McClintock et al. (2006), 4–Gou et al. (2009), 5–Liu et al. (2008, 2010), 6–Shafee et al. (2006), 7–Steiner et al. (2010), 8–Davis et al. (2006), 9–Gou et al. (2010), 10–Fender et al. (2010), 11–Reid et al. (2014), 12–Wu et al. (2016), 13–Chen et al. (2016), 14–Orosz et al. (2014), 15–Steiner et al. (2014)

are used throughout (always appearing inside parentheses), unless stated otherwise. We adopt R_I for the radius of the ISCO,

$$R_S = \frac{2GM}{c^2}, \quad (1)$$

for the Schwarzschild radius, and the dimensionless ratio

$$x \equiv \frac{R_I}{R_S}. \quad (2)$$

Here M represents the BH mass, c is the speed of light, and G is the gravitational constant. The parameter x is a nonlinear function¹ of the dimensionless spin parameter a_* of the BH (Bardeen et al. 1972), where

$$a_* \equiv \frac{cJ}{GM^2}, \quad (3)$$

and J represents the angular momentum of the BH.

The calculations incorporate the equipartition magnetic field B_{eq} derived by Contopoulos & Kazanas (1998) (their eq. [11]) for geometrically thick (ADAF) accretion disks

$$B_{eq} = (9 \times 10^3 \text{ T}) \dot{m}^{0.5} \left(\frac{M}{M_\odot} \right)^{-0.5} x^{-1.25}, \quad (4)$$

where the mass of the BH is scaled in units of the solar mass M_\odot and \dot{m} is the mass accretion rate in units of its Eddington value. This equation provides an estimate of the strongest magnetic field that may be supported throughout the region $R_H \leq R \leq R_I$ between the BH horizon and the ISCO. The value of B_{eq} depends on the location of the ISCO through the $x^{-1.25}$ term, so the ISCO has a say (by as much as a factor of ~ 10) on how much magnetic field will thread the BH horizon. The BH horizon radius R_H is also a nonlinear function of the spin (Bardeen et al. 1972) and we can write (Rieger 2011)

$$R_H = \frac{1}{2} R_S Q_*(a_*), \quad (5)$$

¹ Eq. (2.21) of Bardeen et al. (1972) provides the radius of the “marginally stable orbit” in geometric units as $r_{ms}/M \equiv f_*(a_*)$, where $f_*(a_*)$ is a nonlinear function of the dimensionless spin parameter. For our purposes, r_{ms} is identified with R_I and x is determined from the equation $x = R_I/R_S = f_*(a_*)/2$. We note that this equation does not take into account the more complicated model of Contopoulos & Papadopoulos (2012) in which x depends also on the magnitude of the magnetic field itself.

where

$$Q_*(a_*) \equiv 1 + \sqrt{1 - a_*^2}. \quad (6)$$

For the case of no rotation ($a_* = 0$), the horizon coincides with R_S , whereas in the extreme-rotation case with $a_* = 1$, the horizon shrinks to $R_S/2$. We also need the rotation frequency on the horizon Ω_H at which inertial frames are dragged by the BH at R_H , and this is obtained from the equation (Rieger 2011)

$$\Omega_H R_H = \frac{1}{2} c a_*. \quad (7)$$

As a check, using eqs. (1) and (5), we can cast eq. (7) to the form $\Omega_H = a_*/(2MQ_*)$ in geometric units $c = G = 1$, as was defined by Steiner et al. (2013).

For the poloidal magnetic flux, we find that

$$\begin{aligned} \Psi_{BH} &= B_{eq} (\pi R_H^2) \\ &= (6.2 \times 10^{10} \text{ Wb}) \dot{m}^{0.5} \\ &\quad \times \left(\frac{M}{M_\odot} \right)^{1.5} x^{-1.25} Q_*^2, \end{aligned} \quad (8)$$

and we take the dimensionless flux Ψ_{BH*} to be

$$\Psi_{BH*} \equiv \left(\frac{M}{M_\odot} \right)^{1.5} x^{-1.25} Q_*^2, \quad (9)$$

in units of $(6.2 \times 10^{10} \text{ Wb}) \dot{m}^{0.5}$. This quantity is not directly observable, but it is still useful to examine its behavior in the few stellar-mass BHs that have so far been studied extensively. For this purpose, we adopt an homogeneous data set of 10 BHs (Table 1) whose masses and spins have presently been determined as accurately as possible. The spins were all derived by the CF method. Fig. 1 shows Ψ_{BH*} from eq. (9) vs. a_* for the data listed in Table 1. GRO J1655-40 has smaller mass than neighboring BHs in Fig. 1 and it appears to separate the fluxes into two groups,² one with increased

² There also exists another data set of spins derived by the Fe K α method (Fender et al. 2010; Russell et al. 2013; Reynolds 2014); these data do not disagree with our determinations from the CF data. A similar segregation of objects into two groups is seen in the Fe K α data as well, but a different BH with a markedly small mass is responsible for the gap seen in magnetic fluxes. This BH is XTE J1650-500 with $M = (5 \pm 2.3) M_\odot$ and $a_* = 0.79 \pm 0.01$ (Orosz et al. 2004; Miller et al. 2009; Özel et al. 2010).

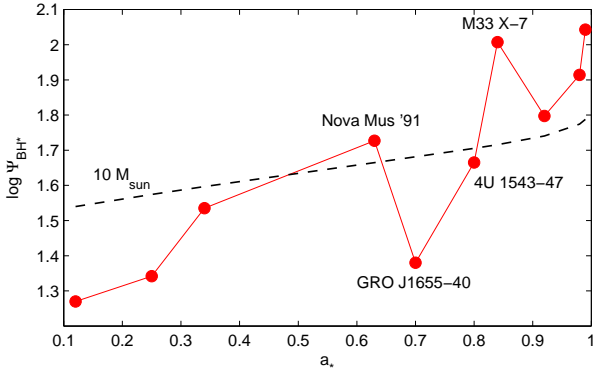


Figure 1. Poloidal magnetic flux Ψ_{BH*} from eq. (9) vs. a_* for the data listed in Table 1 and connected by straight line segments. The dashed line shows a BH with a fixed mass of $10M_\odot$. In order of increasing a_* , the absolute errors in $\log \Psi_{BH*}$ are 0.08, 0.09, 0.11, 0.17, 0.04, 0.08, 0.07, 0.12, 0.12, and 0.06.

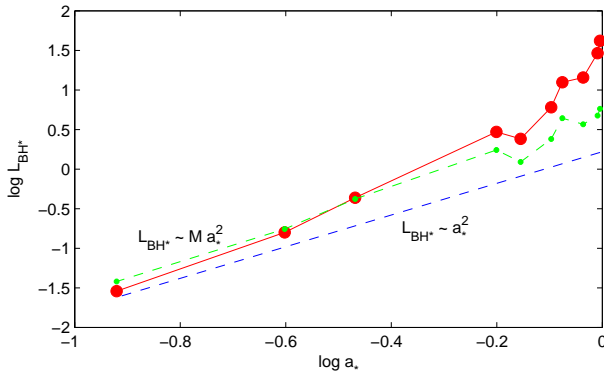


Figure 2. Beam power L_{BH*} from eq. (11) vs. a_* for the data listed in Table 1 and connected by straight line segments. The dashed lines show a pure a_*^2 dependence (blue line) and an Ma_*^2 dependence (green line). The difference between the red and green lines for $\log a_* > -0.2$ ($a_* > 0.63$) shows the strong influence of the magnetic field to the beam power for rapidly spinning BHs. In order of increasing a_* , the absolute errors in $\log L_{BH*}$ are 1.5, 0.65, 0.93, 0.49, 0.13, 0.16, 0.16, 0.28, 0.14, and 0.13.

fluxes at moderate a_* values, and another with the highest fluxes at high a_* values. It is hard to tell whether the effect is significant with so few data available. Nevertheless, we are compelled to consider these two groups separately in the analysis that follows.

For the beam power, we follow Livio et al. (1999) and Meier (1999, 2001), and we find for two outflowing jets that

$$\begin{aligned} L_{BH} &= \frac{1}{2c} B_{eq}^2 R_H^2 (\Omega_H R_H)^2 \\ &= \frac{1}{32} B_{eq}^2 R_S^2 c a_*^2 Q_*^2 \\ &= (6.6 \times 10^{21} \text{ W}) \dot{m} \left(\frac{M}{M_\odot} \right) x^{-2.5} a_*^2 Q_*^2; \end{aligned} \quad (10)$$

then we take the dimensionless beam power L_{BH*} to be:

$$L_{BH*} \equiv \left(\frac{M}{M_\odot} \right) x^{-2.5} a_*^2 Q_*^2, \quad (11)$$

in units of $(6.6 \times 10^{21} \text{ W})\dot{m}$. Fig. 2 shows L_{BH*} from

eq. (11) vs. a_* for the data listed in Table 1. For comparison purposes, fiducial dashed lines show a pure a_*^2 dependence and an Ma_*^2 dependence. In the region with $a_* > 0.63$ ($\log a_* > -0.2$), the actual data rise a lot higher than both dashed lines. This indicates that the beam power does not vary as a_*^2 as is commonly believed. The reason is the strong influence of the $x^{-2.5}$ term which in turn depends on a_* . This influence is most apparent for high a_* values, where the term increases the beam powers substantially (by as much as a factor of 88 compared to the $a_* = 0$ Schwarzschild case); and makes L_{BH*} a much steeper function of a_* than a_*^2 .

As was observed in Fig. 1, the L_{BH*} values in Fig. 2 also segregate into two groups that show different slopes, one at moderate a_* values and another at high a_* values. A linear regression of the lower 4 points with $a_* \leq 0.63$ shows a slope of 2.80 with a correlation coefficient of $r^2 = 0.993$; a linear fit of the higher 6 points with $a_* \geq 0.70$ shows a slope of 7.64 with $r^2 = 0.961$; and a linear fit of all 10 points shows a slope of 3.28 with $r^2 = 0.954$. Therefore, if all the power in the observed transient (ballistic) jets is emitted by the BH alone, the data should show a much steeper slope than the commonly quoted slope of $d \log L_{BH*} / d \log a_* = 2$. In view of these results, the current disagreement on whether such a slope of 2 can be deduced from the existing radio data (Fender et al. 2010; Narayan & McClintock 2012; Russell et al. 2013) appears to be a moot issue. Furthermore, we have calculated that the best-fit line in the Narayan & McClintock (2012) data (after resetting the mass of GRS 1915+105 to the value shown in Table 1) has a slope of $2.66 \pm 0.025(1\sigma)$ which lies within the error bar of our slope of $2.80 \pm 0.17(1\sigma)$ for moderate $a_* \leq 0.7$ where the 3 out of 4 radio sources lie. The next question is whether we can understand the rather perplexing results of Russell et al. (2013) in the context of this investigation. We undertake this task in § 4 below using also Table 2 in which we summarize the above results from linear regressions and the regressions that we describe in subsequent sections.

3 ELECTROMAGNETIC OUTPUT FROM THE BLACK HOLE AND THE INNER DISK

In this section, we add to the results of §2 the contribution from the inner accretion disk. We assume a nonrelativistic accretion flow (Livio et al. 1999; Meier 1999) but we have checked that the results are not modified substantially in the case of a relativistic disk flow (Meier 2001). Again, the calculations incorporate the same equipartition magnetic field B_{eq} (eq. [4]) for the region $R_H \leq R \leq R_I$ between the BH horizon and the ISCO.

The poloidal magnetic flux Ψ now is

$$\begin{aligned} \Psi &= B_{eq} (\pi R_I^2) \\ &= (6.2 \times 10^{10} \text{ Wb}) \dot{m}^{0.5} \left(\frac{M}{M_\odot} \right)^{1.5} (4x^{0.75}), \end{aligned} \quad (12)$$

and we take the dimensionless flux Ψ_* to be:

$$\Psi_* \equiv \left(\frac{M}{M_\odot} \right)^{1.5} (4x^{0.75}), \quad (13)$$

in units of $(6.2 \times 10^{10} \text{ Wb})\dot{m}^{0.5}$. The scaling of Ψ_* is the same as in § 2 in order to facilitate direct comparisons between

Table 2. Summary of Results from Linear Regressions

Power from BH only			
Model	Best-Fit Slope (Correlation r^2)		
	$a_* \leq 0.63$ pts.	$a_* \geq 0.7$ pts.	All 10 points
$L_{BH} \propto a_*^2$	2.80 (0.993)	7.64 (0.961)	3.28 (0.954)
$L_{BH} \propto a_*^4$	4.80 (0.998)	9.64 (0.975)	5.28 (0.982)

Power from Disk and BH			
Model	Best-Fit Slope (Correlation r^2)		
	$a_* \leq 0.63$ pts.	$a_* \geq 0.7$ pts.	All 10 points
$L_{BH} \propto a_*^2$	0.58 (0.903)	4.52 (0.906)	0.92 (0.708)
$L_{BH} \propto a_*^4$	2.58 (0.995)	6.52 (0.953)	2.92 (0.961)

Note.—Statistical 1σ errors in the quoted slopes are ± 0.17 , ± 0.77 , and ± 0.26 (BH only); and ± 0.13 , ± 0.73 , and ± 0.21 (Disk and BH); in each column respectively. A Maximum Likelihood method (York et al. 2004) using the errors listed in Table 1 produces similar results with larger errors in the left two columns, but deviates substantially in the third column where large weights are assigned exclusively to the high a_* points that have small errors (the algorithm is described by Thirumalai et al. 2011). This indicates that a single straight line is not a good fit for all 10 points.

eq. (13) and eq. (9). The parameter x is again related to a_* using the equations of Bardeen et al. (1972).

We adopt again the data set for the 10 BHs listed in Table 1, although we have checked that the data from the Fe K α method do not disagree with our determinations described below. Fig. 3 shows Ψ_* from eq. (13) vs. a_* for the data listed in Table 1. Again GRO J1655-40 appears to separate the fluxes into two groups, one with increased fluxes at moderate a_* values and another at high a_* values. In this case, however, the fluxes at high a_* values are not dominant (compare Fig. 3 to Fig. 1 for $a_* \geq 0.8$). But it is hard to tell whether this division is significant with so few data available. We note that Ψ_* decreases with a_* for a fixed mass such as the $10M_\odot$ BH plotted as a dashed line in Fig. 3. This is the result of the decrease of the disk term $x^{0.75}$ with a_* in eq. (13) and it occurs despite the gradual increase of the contribution from around the BH horizon. Therefore, we have theoretical evidence that the magnetic flux becomes subdued with increasing a_* at high $a_* \geq 0.8$ values when it is dominated by the field lines that thread the inner accretion disk.

For the combined beam power L , we use $v = \sqrt{GM/R_I}$ for the orbital speed of the plasma at the ISCO and we find for two outflowing jets that

$$\begin{aligned}
 L &= L_{Disk} + L_{BH} \\
 &= B_{eq}^2 R_I^2 v + \frac{1}{32} B_{eq}^2 R_S^2 c a_*^2 Q_*^2 \\
 &= (1.5 \times 10^{23} \text{ W}) \dot{m} \left(\frac{M}{M_\odot} \right) x^{-1} \\
 &\quad + (6.6 \times 10^{21} \text{ W}) \dot{m} \left(\frac{M}{M_\odot} \right) x^{-2.5} a_*^2 Q_*^2; \quad (14)
 \end{aligned}$$

then we take the dimensionless beam power L_* to be:

$$L_* \equiv \left(\frac{M}{M_\odot} \right) \left(16\sqrt{2} x^{-1} + x^{-2.5} a_*^2 Q_*^2 \right), \quad (15)$$

in units of $(6.6 \times 10^{21} \text{ W})\dot{m}$. Fig. 4 shows L_* from eq. (15)

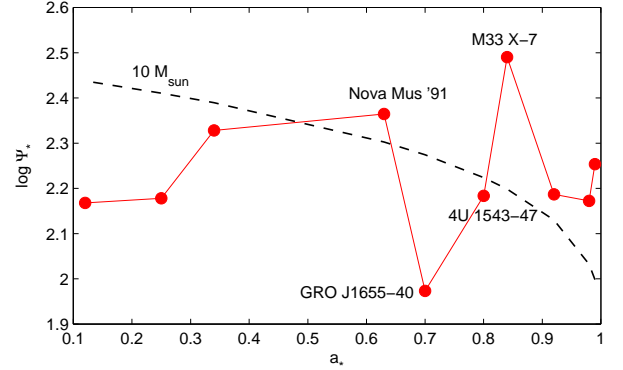


Figure 3. Total poloidal magnetic flux Ψ_* from eq. (13) vs. a_* for the data listed in Table 1 and connected by straight line segments. The dashed line shows the contribution from the disk and a BH with a fixed mass of $10M_\odot$. In order of increasing a_* , the absolute errors in $\log \Psi_*$ are 0.01, 0.02, 0.02, 0.06, 0.01, 0.04, 0.03, 0.01, 0.08, and 0.00.

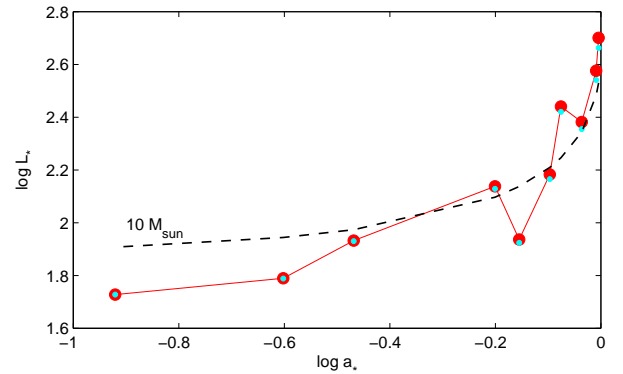


Figure 4. Total beam power L_* from eq. (15) vs. a_* for the data listed in Table 1 and connected by straight line segments. The cyan dots show the disk's contribution to the total power for each object in Table 1. The dashed line shows the combined contribution from the disk and a BH with a fixed mass of $10M_\odot$. In order of increasing a_* , the absolute errors in $\log L_*$ are 0.41, 0.19, 0.24, 0.15, 0.16, 0.17, 0.16, 0.21, 0.09, and 0.05.

vs. a_* for the data listed in Table 1. The L_* values in Fig. 4 can be separated into two groups that show different slopes, one at moderate a_* values and another at high a_* values. A linear regression of the lower 4 points with $a_* \leq 0.63$ shows a slope of 0.58 with a correlation coefficient of $r^2 = 0.903$; a linear fit of the higher 6 points with $a_* \geq 0.70$ shows a slope of 4.52 with $r^2 = 0.906$; and a linear fit of all 10 points shows a slope of 0.92 with $r^2 = 0.708$. The importance of the disk's contribution to the emitted power is apparent in these results. The power from the BH is too small to support the notion that a slope of 2 is significant. Therefore, if the inner accretion disk contributes significantly to compact jet-like poloidal outflows, we expect that the data should show a shallow slope of order $d \log L_*/d \log a_* \approx 0.6 - 0.9$, at least for $a_* < 0.8$ if not for the entire a_* range. In principle, this result does not disagree with the analysis of the observations of continuous compact jets (Fender et al. 2010). Although the data illustrated in Fig. 4 of this study do not show an

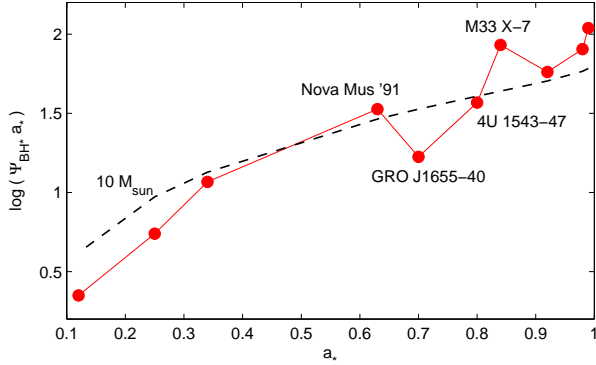


Figure 5. As in Fig. 1, but an additional factor of a_* has been inserted into the flux Ψ_{BH*} in eq. (9). The dashed line shows a BH with a fixed mass of $10M_\odot$. In order of increasing a_* , the absolute errors in $\log(\Psi_{BH*}a_*)$ are 0.76, 0.35, 0.47, 0.29, 0.07, 0.11, 0.10, 0.15, 0.12, and 0.07.

obvious linear correlation, any line that may be fitted will certainly have a very shallow slope. This indicates that the continuous compact jets seen in the hard states of these objects originate mostly from the inner accretion disks and not from the BHs (see also [Kylafis et al. 2012](#)).

4 A NEW ESTIMATE OF THE MAGNETIC FIELD AROUND THE BLACK HOLE

The equations that we have used in the previous sections to estimate the beam power from the BH and the inner nonrelativistic disk are consistent with the jet power expected to be emitted by the BZ mechanism ([Blandford & Znajek 1977](#)) and the BP mechanism ([Blandford & Payne 1982](#); [Contopoulos & Lovelace 1994](#)), respectively ([Livio et al. 1999](#); [Meier 1999](#)). The only novel element in our calculations has been so far the adoption of the equipartition poloidal magnetic field from the work of [Contopoulos & Kazanas \(1998\)](#) on the PRCB (eq. [4]). This equation, along with the location of the ISCO (eq. [2]), has introduced the nonlinear dependence of the beam power on the spin parameter a_* as seen in Figs. 2 and 4. In the case of the BH power, the explicit dependence of L_{BH} on $B_{eq}^2 a_*^2$ that is derived in the BZ mechanism can be seen in eq. (10), and it is the magnetic field that introduces a strong nonlinearity (via the $x^{-2.5}$ term that varies by a factor of 88 from $a_* = 0$ to 1) that spoils the pure a_*^2 dependence in eq. (11) (the term Q_*^2 is not as important as it varies by only a factor of 4). However, these classical equations may not be correct because they assume that the accumulated magnetic field can reach equipartition undisturbed.

The recent work of [Contopoulos et al. \(2016\)](#) indicates that the region $R_H \leq R \leq R_I$ cannot support an equipartition magnetic field unless the BH is maximally rotating ($a_* = 1$). The origin of the problem is the magnetic Rayleigh-Taylor (MRT) instability that allows for the poloidal field to escape by slipping in the azimuthal direction. On the other hand, a fast rotation of the spacetime works toward limiting the instability. A simplified version of the results of [Contopoulos et al. \(2016\)](#) is that the maximum magnetic field that can thread the BH horizon and the

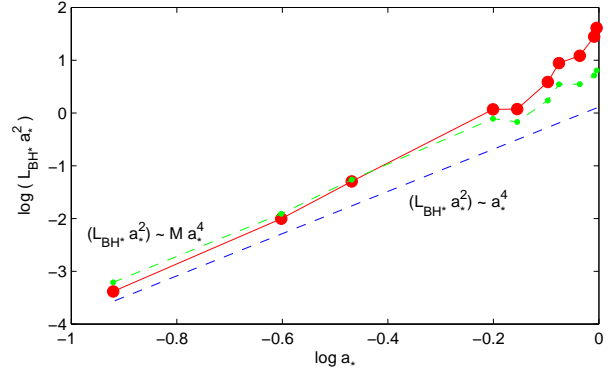


Figure 6. As in Fig. 2, but an additional factor of a_*^2 has been inserted into the power L_{BH*} in eq. (11). The dashed lines show a pure a_*^4 dependence (blue line) and an $M a_*^4$ dependence (green line). The difference between the red and green lines for $\log a_* > -0.2$ ($a_* > 0.63$) shows the strong influence of the magnetic field to the beam power for rapidly spinning BHs. In order of increasing a_* , the absolute errors in $\log(L_{BH*}a_*^2)$ are 2.9, 1.2, 1.6, 0.73, 0.19, 0.22, 0.21, 0.35, 0.14, and 0.14.

inner disk is proportional to the BH spin itself, that is

$$B_{max} \approx B_{eq} a_*, \quad (16)$$

to within factors of order unity. This new result challenges the fundamentals of jet emission from BH binaries (without actually negating the BZ mechanism) and forces us to reconsider the classical picture that was analyzed in §§2 and 3 above. In the following subsections, we adopt eq. (16) to provide a description of the maximum magnetic field around the BH and the inner disk, and we repeat the analyses of §§2 and 3.

4.1 Black Hole

We insert a factor of a_* into Ψ_{BH*} in eq. (9) and a factor of a_*^2 into L_{BH*} in eq. (11). Figs. 5 and 6 are analogous to Figs. 1 and 2 and they show the resulting changes in the physical quantities involved in the emission from the BH only.

The new dependence of B_{max} on the spin parameter has steepened dramatically the slopes of the curves depicted in Figs. 5 and 6. Again, we can separate the results into two groups that show different slopes, one at moderate a_* values and another at high a_* values. By repeating the linear regressions outlined in §2, we find that the new slopes of the best-fit lines to the beam powers now stand higher by +2 while the correlation coefficients are also higher (Table 2). Therefore, if all the power in the observed transient jets is emitted by the BH alone; and if the MRT instability limits the magnetic field around the BH to obey eq. (16); then the radio observations should show dramatically steeper slopes (≈ 5 -10) than the commonly quoted slope of $d \log L_{BH*} / d \log a_* = 2$.

This model may help explain some of the perplexing results obtained by [Russell et al. \(2013\)](#) from radio observations of jets in a large sample of BH binaries. In particular, their Figs. 1c and 1d show clearly two groups of points; one at low/moderate $a_* \leq 0.6$ values with slopes of about 2.5-3 (but still not close to our 4.80); and another at high

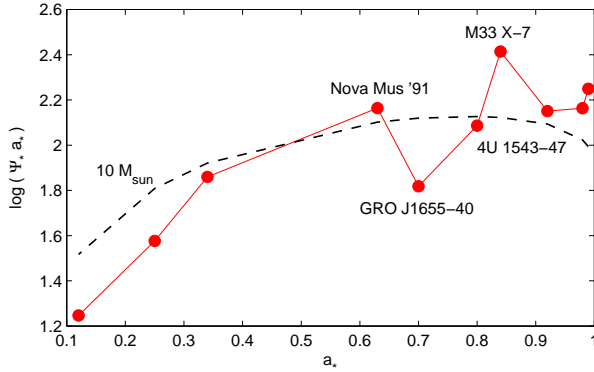


Figure 7. As in Fig. 3, but an additional factor of a_* has been inserted into the flux Ψ_* in eq. (13). The dashed line shows the contribution from the disk and a BH with a fixed mass of $10M_\odot$. In order of increasing a_* , the absolute errors in $\log(\Psi_* a_*)$ are 0.68, 0.28, 0.33, 0.18, 0.04, 0.07, 0.05, 0.05, 0.08, and 0.01.

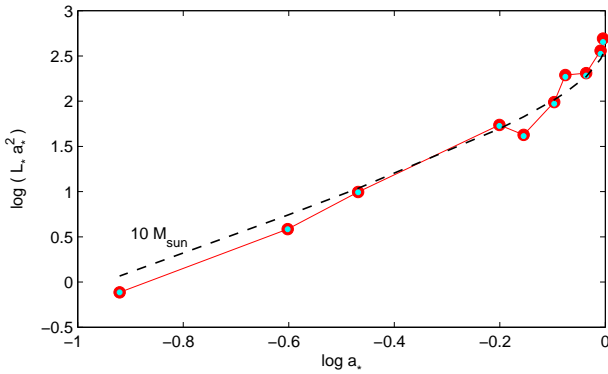


Figure 8. As in Fig. 4, but an additional factor of a_*^2 has been inserted into the power L_* in eq. (15). The cyan dots show the disk's contribution to the total power for each object in Table 1. The dashed line shows the combined contribution from the disk and a BH with a fixed mass of $10M_\odot$. In order of increasing a_* , the absolute errors in $\log(L_* a_*^2)$ are 1.8, 0.71, 0.95, 0.40, 0.22, 0.22, 0.21, 0.28, 0.10, and 0.06.

$a_* \geq 0.63$ values with slopes of about 8-15 (roughly comparable to our 9.64). Given the approximations involved in the radio jet data analysis and in our analysis, we find the rough agreement between these results satisfactory. But we must note that the results of Narayan & McClintock (2012) and Russell et al. (2013) for $a_* \leq 0.63$ seem to support the conventional $L_{BH*} \propto a_*^2$ model of § 2 (see Table 2) and not the new a_*^4 model (but see also § 4.2 and the discussion at the end of § 5 below).

4.2 Accretion Disk and Black Hole

We insert a factor of a_* into Ψ_* in eq. (13) and a factor of a_*^2 into L_* in eq. (15). Figs. 7 and 8 are analogous to Figs. 3 and 4 and they show the resulting changes in the physical quantities involved in the combined emission from the accretion disk and the BH.

By repeating the linear regressions outlined in §3, we find that the new slopes of the best-fit lines to the beam

powers now stand higher by +2 while the correlation coefficients are substantially higher (compare the two bottom rows in Table 2). A surprising element is the linear fit to the lower 4 points ($a_* \leq 0.63$) that produces a line with slope 2.58 and an excellent correlation ($r^2 = 0.995$). This slope is comparable to that of the a_*^2 model with a BH only (2.80; Table 2) and to the slopes seen in the Narayan & McClintock (2012) and Russell et al. (2013) data. As a result, the plot thickens since the emission from dominant a_*^4 disks around moderately spinning BHs appears to have the same signature slope as the power output from a_*^2 BHs surrounded by dormant disks. Theoretical considerations alone cannot tell the difference between these two cases and observations will need to turn to $a_* \geq 0.7$ systems in which active a_*^4 disks are incapable of producing slopes as high as those found for conventional a_*^2 BHs (see the entries for $a_* \geq 0.7$ in Table 2). The $a_* \geq 0.7$ regime appears to also be appropriate for distinguishing between the two a_* models from observations of transient (ballistic) jets. If such jets are produced by rapidly-spinning BHs, then Table 2 indicates that the $d \log L_{BH*} / d \log a_*$ slope predicted by the a_*^4 model is considerably steeper (9.64 as opposed to 7.64 for the a_*^2 model).

5 SUMMARY AND DISCUSSION

In this investigation, we have calculated the physical parameters associated with jet emission from BH binaries, the poloidal magnetic flux and the beam (jet) power. We were aided by an homogeneous data set of BH masses and spins that were determined by the CF method (Table 1). The results do not appear to be modified in a substantial way when we examine data from the Fe K α method or when we adopt relativistic accretion disks, and we opted to not show another set of results for the sake of clarity. Our results can be summarized as follows:

1. The (unobservable) poloidal magnetic flux indicates that the objects may be segregated into two broad groups, one with low/moderate spins, and another with very high spins. This effect is apparent in the classical model (Blandford & Znajek 1977; Blandford & Payne 1982) calculations depicted in Figs. 1 and 3, but it is harder to detect in the new model of jet emission (Contopoulos et al. 2016) shown in Figs. 5 and 7. The two separated groups are created by the particular dependence of the fluxes on the BH masses listed in Table 1. A similar effect is seen in the Fe K α data as well (see footnote 2).
2. The beam power from the vicinity of the BH does not scale with spin as a_*^2 (Fig. 2) because both the location of the ISCO and the supported magnetic field depend nonlinearly on a_* (Bardeen et al. 1972; Contopoulos & Kazanas 1998; Contopoulos & Papadopoulos 2012). Linear fits to the data indicate that the actual scaling is steeper and closer to 2.8-3.3 for most of the range of a_* values and close to 7.6 for high a_* values (§ 2, Table 2). In view of these results, the controversy that has developed about the a_*^2 scaling (Fender et al. 2010; Narayan & McClintock 2012; Russell et al. 2013) now appears to be moot. Interestingly, both sets of results can now be interpreted in a consistent manner (see the discussions at the end of § 2 and at the end of § 4.1).
3. When the contribution of the inner accretion disk is included, the disk power output dominates over the output

produced near the BH (§ 3, Figs. 3 and 4). Then, linear fits to the data listed in Table 2 indicate that the actual scaling of the beam power is quite shallow ($d \log L_*/d \log a_* \approx 0.6-0.9$ at least over the interval of $0 \leq a_* < 0.8$).

4. A new model of jet power, the a_*^4 model (Contopoulos et al. 2016), was outlined in § 4; as shown in Table 2, it predicts higher slopes (by an additional +2) in various sections of the data relative to the slopes determined for the conventional a_*^2 -power models. Interestingly, very steep slopes were found also by Russell et al. (2013) in the high a_* regime when they analyzed the available radio observations of BH transient (ballistic) jets.

5. The current observational data (Narayan & McClintock 2012; Russell et al. 2013) for systems with moderate $a_* \leq 0.63$ values do not let us distinguish between the two a_* models or between emission from a dominant a_*^2 BH versus from an a_*^4 BH with a dominant inner accretion disk. The results discussed in § 4.2 indicate that observations of jets from rapidly-spinning BHs ($a_* \geq 0.7$) may help us resolve both of these issues in the future, but it will not be easy: in the former case, the difference between slopes is only +2 in all cases and in all a_* intervals; and in the latter case, the slopes differ only by about +1 (a slope of 7.64 vs. 6.52 in Table 2).

The steep dependence of the power output on a_* seen in Table 2 for $a_* \geq 0.7$ has also been seen in simulated relativistic models of BHs accreting from surrounding ADAF-type disks. For BH jets and for $a_* > 0.5$, McKinney (2005) found that the best-fit slope was 5 whereas Tchekhovskoy et al. (2010) found values as high as 6 for the thickest of their ADAF models with $a_* > 0.7$. These results seem to point in the right direction, but they still lie below our most conservative slope (7.64; Table 2). Furthermore, McKinney (2005) obtained a fit to the total power output in these models and a slope of 4. This result points again in the right direction: Table 2 shows that the slope of the total power decreases by about 3 units compared to the pure BH power. In this case, the slope of 4 of McKinney (2005) appears to compare favorably with our slope of 4.52 derived from the a_*^2 BH model with a dominant accretion disk.

On the other hand, the steep slope of 4.80 found in the new a_*^4 BH model (§ 4.1) for $a_* \leq 0.63$ is not borne out by the analyses of radio observations of Narayan & McClintock (2012) and Russell et al. (2013) that indicate typical slopes of about 2.5-3. These studies show that, in low a_* objects, the ballistic jet power does not decrease with decreasing a_* as strongly as implied by the a_*^4 BH model. We have tried to understand this outcome as follows: In the a_*^4 BH model (Contopoulos et al. 2016), the MRT instability limits the accumulated magnetic field B_{max} to a value well below the equipartition value B_{eq} in low a_* objects (eq. [16]), but this will not be reflected in the data if the magnetic field is continually produced by the PRCB and the accretion occurs on dynamical (free-fall) timescales. The MRT instability also acts dynamically to remove the accumulated magnetic flux near the BH. One may then argue that for half the time, the flux is brought into the vicinity of the BH from the ISCO; and for the other half, a fraction of the flux, proportional to $(1 - a_*)B_{eq}$, is removed from the same area. As a result, the average (integrated over time and divided by the total time interval) accumulated mag-

netic field will not decrease to that given by eq. (16) which is stable against the MRT instability; but it will remain instead near the time-integrated average value that is proportional to $(1 + a_*)B_{eq}/2$. This estimate yields the expected behavior for $a_* \rightarrow 1$ ($B_{max} \rightarrow B_{eq}$); but for $a_* \rightarrow 0$, it shows that a substantial fraction of the equipartition magnetic field ($B_{eq}/2$) will remain near the BH horizon. In this case (of “the $(1 + a_*)^2 a_*^2/4$ model”), a linear regression to the objects of Table 1 with $a_* \leq 0.63$ shows a slope of 3.25 ($r^2 = 0.990$) as opposed to the slope of 4.80 listed in the second row of Table 2.

ACKNOWLEDGMENTS

We thank the referee whose comments led to a thorough analysis of the error bars in our calculations. DMC and SGTL were supported in part by NASA grant NNX14-AF77G. DK was supported by a NASA ADAP grant. JFS was supported by NASA Einstein Fellowship grant PF5-160144.

REFERENCES

- Bardeen, J. M., Press, W. H., & Teukolsky, S. A. 1972, *ApJ*, 178, 347
- Blandford, R. D., & Payne, D. G. 1982, *MNRAS*, 199, 883
- Blandford, R. D., & Znajek, R. L. 1977, *MNRAS*, 179, 433
- Blum, J. L., Miller, J. M., Fabian, A. C., et al. 2009, *ApJ*, 706, 60
- Chen, Z., Gou, L., McClintock, J. E., et al. 2016, *ApJ*, submitted, arXiv: 1601.00615
- Christodoulou, D. M., Contopoulos, I., & Kazanas, D. 2008, *ApJ*, 674, 388
- Christodoulou, D. M., Gabuzda, D. C., Contopoulos, I., & Kazanas, D. 2016, *A&A*, in press
- Contopoulos, I., Christodoulou, D. M., Kazanas, D., & Gabuzda, D. C. 2009, *ApJL*, 702, L148
- Contopoulos, I., & Kazanas, D. 1998, *ApJ*, 508, 859
- Contopoulos, I., Kazanas, D., & Christodoulou, D. M. 2006, *ApJ*, 652, 1451
- Contopoulos, I., Kazanas, D., & Papadopoulos, D. B. 2016, *MNRAS*, submitted
- Contopoulos, J., & Lovelace, R. V. E. 1994, *ApJ*, 429, 139
- Contopoulos, I., & Papadopoulos, D. B. 2012, *MNRAS*, 425, 147
- Davis, S. W., Done, C., & Blaes, O. M. 2006, *ApJ*, 647, 525
- Fender, R. P., Gallo, E., & Russell, D. 2010, *MNRAS*, 406, 1425
- Gou, L., McClintock, J. E., Liu, J., et al. 2009, *ApJ*, 701, 1076
- Gou, L., McClintock, J. E., Reid, M. J., et al. 2011, *ApJ*, 742, 85
- Gou, L., McClintock, J. E., Steiner, J. F., et al. 2010, *ApJ*, 718, L122
- Hiemstra, B., Méndez, M., Done, C., et al. 2010, *MNRAS*, 411, 137
- Kolehmainen, M., & Done, C. 2010, *MNRAS*, 406, 2206
- Kylafis, N. D., Contopoulos, I., Kazanas, D., & Christodoulou, D. M. 2012, *A&A*, 538, A5
- Liu, J., McClintock, J. E., Narayan, R., et al. 2008, *ApJ*, 679, L37
- Liu, J., McClintock, J. E., Narayan, R., et al. 2010, *ApJ*, 719, L109
- Livio, M., Ogilvie, G. I., & Pringle, J. E. 1999, *ApJ*, 512, 100
- McClintock, J. E., Narayan, R., Davis, S. W., et al. 2011, in *Classical and Quantum Gravity*, GR19, eds. D. Marolf & D. Sudarsky
- McClintock, J. E., Narayan, R., & Steiner, J. F. 2014, *Sp. Sci. Rev.*, 183, 295

- McClintock, J. E., Shafee, R., Narayan, R., et al. 2006, *ApJ*, 652, 518
- McKinney, J. C. 2005, *ApJ*, 630, L5
- Meier, D. L. 1999, *ApJ*, 522, 753
- Meier, D. L. 2001, *ApJ*, 548, L9
- Miller, J. M. 2007, *ARA&A*, 45, 441
- Miller, J. M., Miller, M. C., & Reynolds, C. S. 2011, *ApJ*, 731, L5
- Miller, J. M., Reynolds, C. S., Fabian, A. C., et al. 2009, *ApJ*, 697, 900
- Narayan, R., & McClintock, J. E. 2012, *MNRAS*, 419, L69
- Orosz, J. A., McClintock, Aufdenberg, J. P., et al. 2011, *ApJ*, 742, 84
- Orosz, J. A., McClintock, J. E., Remillard, R. A., & Corbel, S. 2004, *ApJ*, 616, 376
- Orosz, J. A., Steiner, J. F., McClintock, J. E., et al. 2014, *ApJ*, 794, 154
- Özel, F., Psaltis, D., Narayan, R., & McClintock, J. E. 2010, *ApJ*, 725, 1918
- Reid, M. J., McClintock, J. E., Steiner, J. F., et al. 2014, *ApJ*, 796, 2
- Reis, R. C., Fabian, A. C., Ross, R. R., & Miller, J. M., 2009, *MNRAS*, 395, 1257
- Reis, R. C., Miller, J. M., Fabian, A. C., et al. 2010, *MNRAS*, 410, 2497
- Remillard, R. A., & McClintock, J. E. 2006, *ARA&A*, 44, 49
- Reynolds, C. S. 2014, *Sp. Sci. Rev.*, 183, 277
- Rieger, F. M. 2011, *Int. J. Mod. Phys. D*, 20, 1547
- Russell, D. M., Gallo, E., & Fender, R. P. 2013, *MNRAS*, 431, 405
- Shafee, R., McClintock, J. E., Narayan, R., et al. 2006, *ApJ*, 636, L113
- Shaposhnikov, N., & Titarchuk, L. 2009, *ApJ*, 699, 1223
- Steiner, J. F., McClintock, J. E., & Narayan, R. 2013, *ApJ*, 762, 104
- Steiner, J. F., McClintock, J. E., Orosz, J. A. 2014, *ApJ*, 793, L29
- Steiner, J. F., Reis, R. C., McClintock, J. E., et al. 2010, *MNRAS*, 416, 941
- Tchekhovskoy, A., Narayan, R., & McKinney, J. C. 2010, *ApJ*, 711, 50
- Thirumalai, K., Singh, A., & Ramesh, R. 2011, *J. Geological Soc. India*, 77, 377
- Wu, J., Orosz, J. A., McClintock, J. E., et al. 2016, *ApJ*, submitted, arXiv: 1601.00616
- York, D., Evensen, N. M., López Martínez, M., & De Basabe Delgado, J. 2004, *Am. J. Phys.*, 72, 367